

# Recent Advances and Design Strategies Towards Wearable Near-Infrared Spectroscopy

SHUOYAN LIU<sup>1</sup>, BING XUE<sup>1</sup>, WENYUAN YAN<sup>2</sup>, ALINA Y. RWEI<sup>3</sup>, AND CHANGSHENG WU<sup>1,4,5</sup> 

<sup>1</sup>Department of Materials Science and Engineering, National University of Singapore, Singapore 117575

<sup>2</sup>Department of Materials Science and Engineering, Northwestern University, Evanston, IL 60208 USA

<sup>3</sup>Department of Chemical Engineering, Delft University of Technology, 2629 Delft, HZ, The Netherlands

<sup>4</sup>Institute for Health Innovation and Technology, National University of Singapore, Singapore 117599

<sup>5</sup>The N.1 Institute for Health, National University of Singapore, Singapore 117456

CORRESPONDING AUTHOR: CHANGSHENG WU (e-mail: cwu@nus.edu.sg)

This work was supported by the National University of Singapore Presidential Young Professorship Start-Up Grant.

**ABSTRACT** With a growing focus on properties of softness, miniaturization, and intelligence, extensive research has been focusing on constructing wearable electronic devices facilitating comfort, wearable health monitoring and diagnosis. Among recent progress in the development of wearable bioelectronics, wearable near-infrared spectroscopy (NIRS) devices demonstrate wide implementation possibilities in multiple health monitoring scenarios. Throughout the years, multiple design strategies have assisted in developing wearable NIRS devices with high wearing comfortability and miniaturized size. This review summarizes the principle of NIRS technology, recent advances in design strategies towards soft, wearable, miniaturized NIRS devices, and the future potential development directions. Based on the discussion of different design strategies, including modular device design, flexible hybrid electronics, and materials innovation, we also pinpoint some development directions for wearable NIRS. The reviewed and proposed research efforts may enhance the applicability and capability of NIRS as an important technology for digital health.

**INDEX TERMS** Functional near-infrared spectroscopy, infrared sensors, optical sensors, wearable sensors, wireless sensor networks.

## I. INTRODUCTION

With the advances in electronics, materials, and manufacturing, health monitoring devices are evolving towards increased wearability with smaller sizes. However, challenges still exist in wearable device design. The traditional design implements rigid printed circuit boards (PCB) with hard electrical components [1], [2], [3], bringing low device wearing comfort not suitable for long-term wearing applications. The mismatch between rigid devices and soft human skin could negatively influence monitoring accuracy. The abovementioned challenges reveal the importance of developing soft, lightweight, and wearable electronics.

Near-infrared spectroscopy (NIRS) is a spectroscopic technology employing near-infrared (NIR) light for physiological monitoring, including oxygenation status [4], [5], heart rate [6], [7], vascular tone [8], [9], pulse wave velocity [10], [11], and blood pressure [12], [13]. Since the development of the first NIRS device in 1977 [14], researchers have been

working to utilize various design strategies, structures, and advanced manufacturing processes for the development of soft, miniaturized NIRS devices. A series of design strategies have been proposed to accommodate the challenges faced in constructing these devices. For example, implementing modular device design increases the limited sensing areas caused by the miniaturized sizes of these devices, while other strategies involving flexible hybrid electronics (FHE) technology and materials innovation aims at improving the overall flexibility and softness of the devices.

In this review, we aim to summarize emerging design strategies of wearable NIRS devices over recent years. Starting with the introduction of fundamental principles of NIRS, we categorize recent development efforts of wearable NIRS devices into three different design strategies, i.e., modular device design [15], FHE [16], and materials innovation [17] (Fig. 1(a)).

Modular device design refers to the development of small sensing modules that can be integrated in a reconfigurable

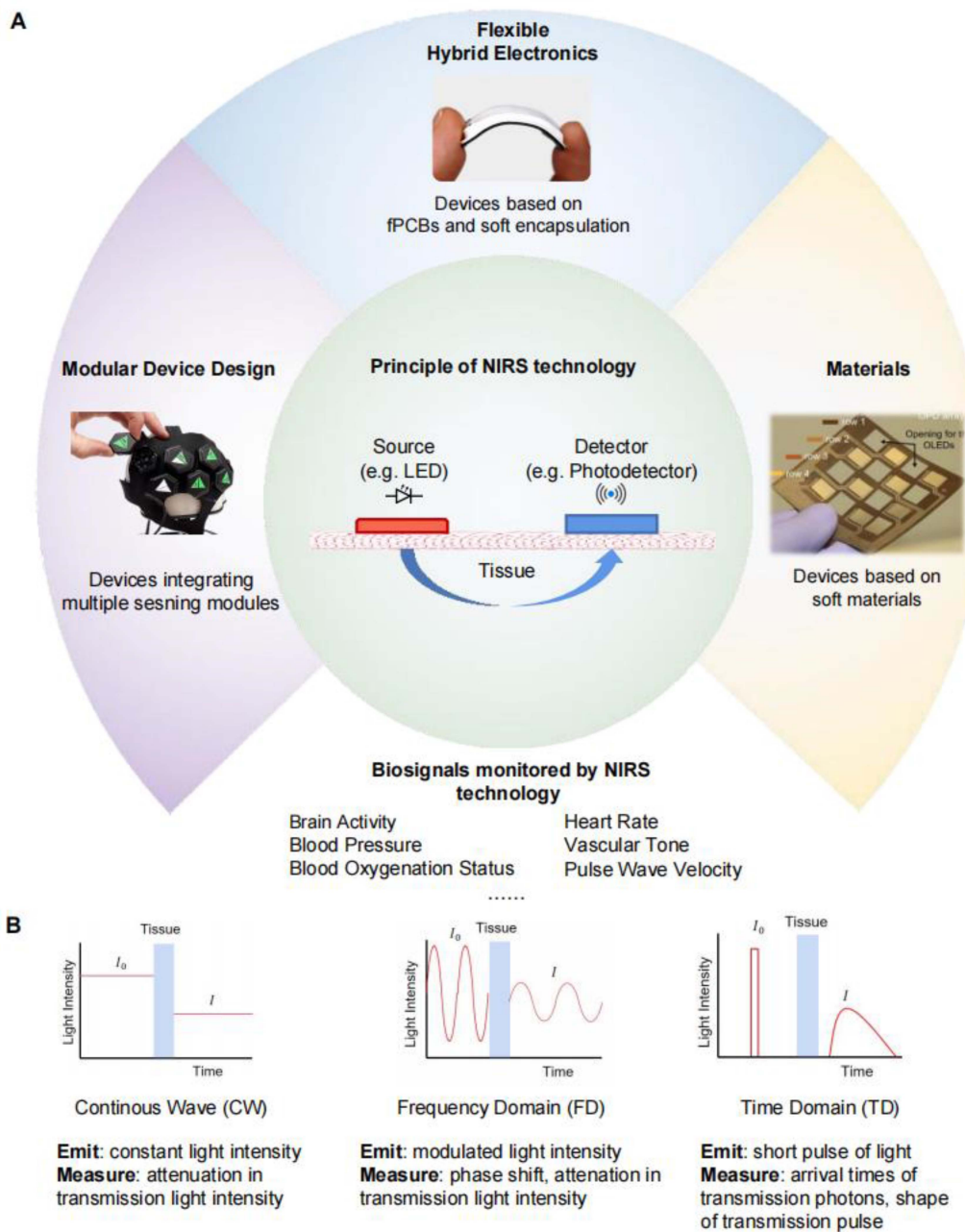


**FIGURE 1. Overview of NIRS technology and strategies towards NIRS device design. (a) NIRS technology principle (the inner circle). Three strategies towards constructing wearable, soft, miniaturized NIRS devices (the outer circle): modular device design strategy [15] (figure reproduced under the terms of the CC BY 4.0 License. Copyright 2020, Elsevier), flexible hybrid electronics [16] (figure reproduced under the terms of the CC BY-NC-ND 4.0 License. Copyright 2020, NAS), and materials innovation [17] (figure reproduced under the terms of the CC BY-NC-ND 4.0 License. Copyright 2018, NAS). (b) Principle schematic of three different categories of NIRS devices (CW, FD, TD) [19].**

or high-density way to allow on-demand and high-resolution measurement for varied areas and anatomies. FHE combines soft encapsulation materials with rigid components and structurally optimized flexible printed circuit boards (fPCBs) to improve softness and wearability. Materials innovation aims at developing intrinsically flexible sensing elements, e.g., light emitting diodes (LEDs) and photodetectors (PDs), for maximum softness and flexibility. We first introduce the detailed design methodology in each strategy, followed by selected

examples demonstrating practical implementations and applications. Based on the strategies discussed above, we finally provide an outlook for developing future wearable NIRS devices.

## II. PRINCIPLES OF NIRS

NIRS is a light-based technology using near-infrared (NIR) radiation of the electromagnetic spectrum to achieve biosignal monitoring. NIRS technology utilizes light sources to emit

NIR light into target tissues and detectors to measure the intensity of penetrated light from the tissues. Chromophores in tissues, such as oxygenated hemoglobin ( $O_2Hb$ ) and deoxygenated hemoglobin ( $HHb$ ), exhibit different optical absorption properties under NIR light (i.e., with a wavelength of 650–1000 nm) [18], causing a difference between the emitted and detected light intensity upon changes in tissue oxygenation. Therefore, NIRS enables quantitative monitoring of important physiological parameters, including the concentrations of  $O_2Hb$ ,  $HHb$ , and total hemoglobin ( $[tHb]=[O_2Hb]+[HHb]$ ). These parameters provide insights into blood perfusion for cerebral, muscle, and cardiac monitoring, making NIRS an attractive technology in both diagnostic and preventive healthcare.

Generally, NIRS devices consist of NIR laser diodes or LEDs as light sources and photodetectors to detect the transmitted light (Fig. 1(a)). They can be classified into three major categories: continuous wave (CW), frequency domain (FD), and time domain (TD) (Fig. 1(b)). CW devices measure the changes in the intensity of the re-emerging light when emitting light at a constant intensity. FD and TD are time-resolved techniques that measure both the light intensity and the time of flight [19]. In FD devices, LED sources modulate the emitted light intensity, and the detector measures phase shift corresponding to the flight time. In TD devices, LED sources emit a short pulse of light into the tissue while the detector measures the arrival times of the re-emerged photons. Despite the higher sensing accuracy of FD and TD, the increased device complexity and relatively high costs prevent FD- and TD-based devices from large-scale commercial applications. Therefore, most commercial NIRS devices are based on CW [19].

Early NIRS devices usually embody a simple structure based on evenly paired light sources and detectors, forming a single source-detector distance [20], [21]. These devices with a single distance have a low measurement accuracy, and could be easily influenced by the outer layers of tissues [22]. Later research [23] indicated that increasing the source-detector distance could enable higher depth sensitivity. Therefore, utilizing multiple source-detector distances could provide enhanced monitoring performance.

The Modified Beer-Lambert law (MBLL) enables the derivation of  $[O_2Hb]$ ,  $[HHb]$ , and  $[tHb]$  from the measured light intensity data [24]. It gives the relationship between light intensity loss (optical density,  $OD$ ) and the molar extinction coefficients ( $\varepsilon$ ), chromophore concentrations ( $c$ ), differential path length factor ( $DPF$ ), source-detector distance ( $d$ ), and the light intensity loss parameter caused by scattering ( $G$ ), as shown by (1):

$$OD(t, \lambda) = -\log\left(\frac{I(t, \lambda)}{I_0(t, \lambda)}\right) = \sum_i \varepsilon_i(\lambda)c_i(t)DPF(\lambda)d + G(\lambda) \quad (1)$$

where  $I_0$ ,  $I$  represent the emitted and detected light intensity, and  $i$  refers to the target chromophores, such as  $[O_2Hb]$

and  $[HHb]$ . Previous research revealed that the value of  $DPF$  varies with age and gender [19], [25], [26], [27]. From (1), the concentration changes of hemoglobin ( $\Delta[HHb]$  and  $\Delta[O_2Hb]$ ) can be solved as:

$$\begin{bmatrix} \Delta[HHb] \\ \Delta[O_2Hb] \end{bmatrix} = \frac{1}{d} \begin{bmatrix} \varepsilon_{HHb, \lambda_1} & \varepsilon_{O_2Hb, \lambda_1} \\ \varepsilon_{HHb, \lambda_2} & \varepsilon_{O_2Hb, \lambda_2} \end{bmatrix}^{-1} \begin{bmatrix} \frac{\Delta OD(\Delta t, \lambda_1)}{DPF(\lambda_1)} \\ \frac{\Delta OD(\Delta t, \lambda_2)}{DPF(\lambda_2)} \end{bmatrix} \quad (2)$$

where  $\lambda_1$  and  $\lambda_2$  are the respective wavelengths.

However, MBLL could not give the absolute values of  $[HHb]$  and  $[O_2Hb]$ , but only their changes [28]. One way to improve the accuracy of the measurement is to consider partial differential pathlength [29] when performing the calculation.

The use of multiple source-detector distances enables the calculation of  $[HHb]$  and  $[O_2Hb]$  based on spatial approaches, including spatially resolved spectroscopy (SRS) [30], [31] and self-calibrating (SC) [32], [33] methods. Spatial algorithms implement several source-detector distances to measure the target tissue simultaneously, determining absolute values of  $[HHb]$  and  $[O_2Hb]$ . Compared to the MBLL algorithm mentioned above, spatial approaches can estimate absolute values of target signals, which are more robust against motion artifacts [19]. The method of SRS utilizes at least two source-detector distances, and the method of SC employs at least two symmetrically arranged sources and detectors, compensating for time-varying differences in light coupling [32]. The source-detector distance varies in accordance with the actual measuring region and light wavelengths [34].

Based on the values of  $[HHb]$  and  $[O_2Hb]$ , the tissue oxygen saturation ( $StO_2$ ) can be calculated as:

$$StO_2 = \frac{[O_2Hb]}{[O_2Hb] + [HHb]} \quad (3)$$

Notably, NIRS shares many similarities with pulse oximetry, especially in hardware design, but their sampling targets and calculations are different. NIRS measures the changes in  $[HHb]$  and  $[O_2Hb]$  in a local tissue with contributions from both arterial and venous blood, while pulse oximetry calculates the peripheral oxygen saturation ( $SpO_2$ ) in the arterial blood. As the arterial blood volume fluctuates periodically with cardiac movement while the venous and capillary blood volume remains relatively stable, detected signals consist of two components: alternating current (AC) component contributed by arterial blood and direct current (DC) component contributed by venous, capillary blood, and tissues. NIRS uses the DC component for the calculation of optical density and  $StO_2$ , while pulse oximetry uses the ratio of AC and DC components for the calculation of  $SpO_2$ .

### III. DEVELOPMENT OF COMMERCIAL NIRS DEVICES

Since the emergence of the first NIRS device, companies and research institutions have constructed extensive commercial NIRS systems [35], [36], [37], [38], [39], ranging from portable systems containing few sources and detectors to bulky systems covering large monitoring areas. The prices of these systems vary from ten thousand to hundred thousand US dollars [19].

In 1977, Frans Jobsis first demonstrated continuous and non-invasive monitoring of the [O<sub>2</sub>Hb] and [HHb] in the brain using NIRS [14]. The prototypes of commercial NIRS devices emerged from 1980 to 1995, under the active cooperation between companies and research institutions, for example, American Edwards Laboratories and Duke University [34]. The first TD NIRS device was proposed by Deply et al. [40] from the University College London in 1988, while Gratton et al. [34], [41] reported the first FD measurements for tissue sensing in 1990. Based on the four-wavelength system proposed by Cope et al. [42] in 1988, a single-channel CW NIRO-1000 NIRS device was built in 1989, marking the successful construction of the first commercial system. Shimadzu created the first commercial single-channel oximeter (OM-200) using SRS in 1997, followed by the introduction of two-channel SRS oximeters (NIRO-300 (Hamamatsu) and INVOS-4100 (Somanetics)) in 1998 [34].

With years of development, commercial NIRS devices have been evolving from bulky wired devices [43], [44], [45], [46] requiring professional operations to wireless devices [47], [48], [49] facilitating comfortable wearable monitoring of target biosignals. In the following sections, we will discuss different design strategies of recent developments leading to the future of constructing wearable, soft, miniaturized NIRS devices.

#### IV. STRATEGIES TOWARDS WEARABLE, SOFT, MINIATURIZED NIRS DEVICES

Recent development in wearable NIRS devices can be categorized into three design strategies: modular device design, FHE, and materials innovation. The modular device design enables reconfiguration and high-density integration of multiple sensing modules to achieve on-demand, high-resolution measurements for varied areas and anatomies. FHE combines soft encapsulation materials with rigid components and structurally optimized fPCBs to improve softness and wearability. Materials innovation focuses on developing intrinsically soft materials to construct fully flexible devices. Due to the close similarity in hardware design between NIRS and pulse oximetry, in this section, some NIR devices developed for pulse oximeters which are insightful for NIRS development are also included.

##### A. MODULAR DEVICE DESIGN

Many previous efforts [50], [51], [52] reported wearable NIRS devices based on small rigid PCBs. To enable on-demand and high-resolution sensing for varied areas and anatomies, NIRS systems consisting of reconfigurable and high-density small sensing modules have been proposed.

Primary efforts include combining multiple identical individual NIRS sensing modules into one system. For example, Guo et al. [53] reported a multi-channel compact-size wireless hybrid surface electromyography (sEMG)-NIRS system to simultaneously acquire muscle electrophysiological, hemodynamic, and oxidative metabolic information. The system consists of four NIRS modules and can be employed on four

different positions on the forearm (Fig. 2(a) and (b)). The hybrid system provides multimodal information about muscle activation, including electrophysiology, hemodynamics, and oxidative metabolism, to reveal fatigue mechanisms in arm amputation patients.

The modular design of a system is not limited to combining several identical NIRS sensors. Gajos et al. [54] designed a NIRS sensing bracelet consisting of 14 modules that can be placed around wrists for high-accuracy hand gesture recognition. Every module of the bracelet contains a light source and a detector placed in rubber holes facilitating the stretching and bending of the bracelet.

The high-density combination of NIRS sensors forming optical arrays brings possibilities to diffuse optical tomography (DOT). By implementing multiple light sources and detectors, DOT provides a better spatial sampling of the target object compared to ordinary NIRS sensors to achieve higher spatial localization and depth investigation capabilities. Chiarelli et al. [55] built a fibreless, multi-channel NIRS-electroencephalogram (EEG) system with multiple bicolor LEDs and silicon photomultipliers (SiPM) mounted onto a commercial EEG cap, forming a high-density optical array for monitoring the brain activity of Alzheimer's Disease patients (Fig. 2(d) and (e)).

High-density DOT (HD-DOT) uses more sources and detectors to provide improved spatial resolution and specificity compared to DOT and ordinary NIRS sensors. A compact array can be constructed using multiple HD-DOT modules by overlapping measurements between several source-detector pairs to obtain different depths and location information of a certain area [56]. Zhao et al. [57] proposed a wearable, modular, rigid-flexible HD-DOT device based on two different connection types (dual-hexagon and tri-hexagon) of LUMO modules (Gowerlabs Ltd., U.K.) for sensorimotor imaging, which enables a flexible NIRS array to construct three-dimensional images of the target object (Fig. 2(f)). Based on the same LUMO module, Frijia et al. [15] built a NIRS sensing cap for infant cerebral monitoring using neoprene, constructing a high-friction, rubberized surface. Twelve independent LUMO modules located in two halves of the cap and connected by straps facilitate a smooth fit for different head sizes and shapes (Fig. 2(g)). Despite the benefit of increased sampling density, the increased number of channels in HD-DOT also makes the construction of wearable devices more challenging [57].

##### B. FLEXIBLE HYBRID ELECTRONICS

Another important design strategy of NIRS devices is FHE. With recent progress in soft materials, device manufacturing and electronic design, this strategy is experiencing rapid development, laying a solid foundation for soft, miniaturized biosensors [58]. FHE utilizes fPCB with rationally designed stretchable structures like serpentines to facilitate high ductility. These devices are encapsulated by soft materials, like medical-grade silicone elastomer [16], [59], featuring

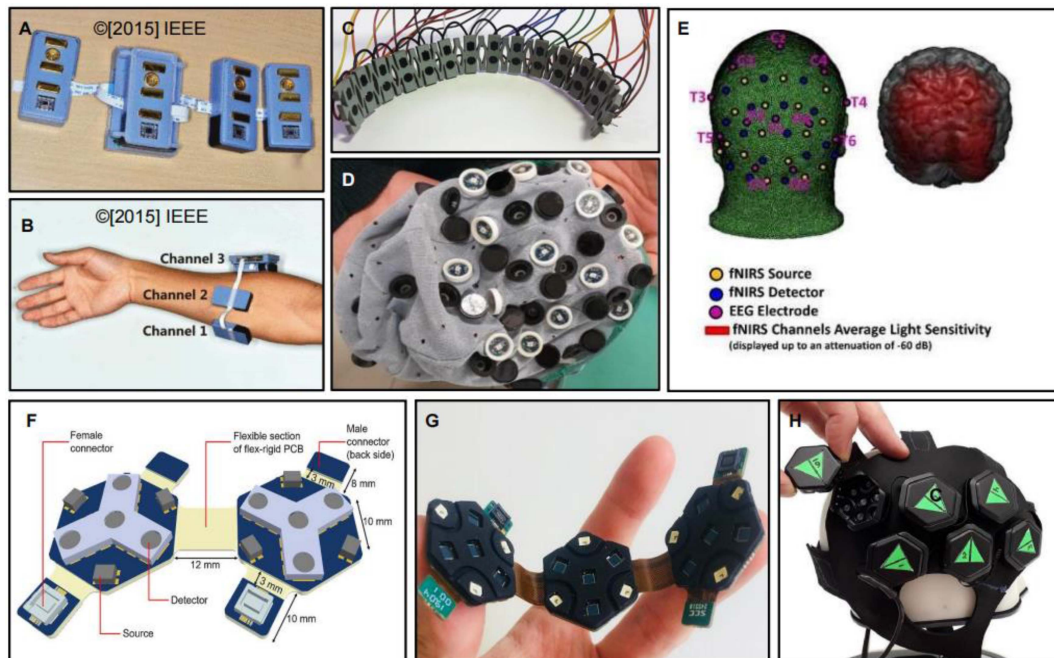


**FIGURE 2.** Wearable NIRS devices based on modular device design. (a-b) Four-channel hybrid sEMG/NIRS system for simultaneous acquisition of muscle electrophysiological, hemodynamic, and oxidative metabolic information. (a) Prototype of the system. (b) Placement of the sensors on 4 positions over the forearm. [53] Reproduced with permission. Copyright 2015, IEEE. (c) The gesture sensing bracelet made of 14 sensing modules. [54] Reproduced with permission. Copyright 2017, ACM. (d-e) Fibreless, multi-channel fNIRS-EEG system forming a high-density optical array for brain activity monitoring. (d) Photo of the NIRS-EEG cap. (e) Configuration of fNIRS optodes and EEG electrodes. [55] Reproduced under the terms of the CC BY 4.0 License. Publisher: MDPI. (f-g) Wearable, modular, rigid-flexible HD-DOT device based on LUMO module for sensorimotor imaging. (f) Dual-hexagon configuration. (g) Triple-hexagon configuration. [57] Reproduced under the terms of the CC BY 4.0 License. Copyright 2017, SPIE. (h) NIRS sensing cap for infant cerebral monitoring using 12 LUMO modules. [15] Reproduced under the terms of the CC BY 4.0 License. Publisher: Elsevier.

a conformable skin interface and thin, waterproof device protection. FHE can significantly improve the wearability of NIRS devices, including continuous health monitoring even in non-clinical settings [16].

In this section, we review selected FHE-based devices and categorize them into two groups based on the number of source-detector distances in the devices. Earlier efforts of FHE-based devices implement single source-detector distance with one detector. In 2016, Kim et al. [59] proposed a wireless, battery-free active optoelectronic system encapsulated with thin, stretchable silicone film. The device could achieve multiple sensing modalities, including the monitoring of heart rate, temporal dynamics of arterial blood flow and tissue oxygenation, as well as enabling ultraviolet (UV) dosimetry and four-color spectroscopic skin evaluation to facilitate both hospital care and at-home diagnostics of various diseases. The sensing modality varies with the wavelengths of the light sources. For example, the device with an infrared (950 nm) LED and a silicon photodetector could monitor heart rate. The addition of a red (625nm) LED measures tissue oxygenation and its temporal variations. Adding UV-responsive dye to the encapsulation of the device enables UV dosimetry. Skin color assessment, realized by mounting four LEDs (infrared, red, orange, and yellow) on the platform, could monitor skin-color-related diseases like hyperbilirubinemia, acute bilirubin encephalopathy, hemochromatosis, and Addison's disease (Fig. 3(a)–(d)).

Zhang et al. [60] constructed a wireless and fully implantable probe incorporating microscale optoelectronics to continuously sense local hemoglobin dynamics by analyzing regional tissue oxygen saturation levels (rStO<sub>2</sub>). Consisting of an injectable filament and a thin, battery-free module, the system is fabricated using micro-transfer printing with elastomeric stamps made from polydimethylsiloxane (PDMS) to enable precise assembly of two microscale LEDs ( $\mu$ -LEDs) and one microscale PD ( $\mu$ -PD). Photolithographically defined traces interconnect the components onto a substrate of polyimide (Fig. 3(e)).

Lu et al. [61] proposed a high-performance, patient-friendly implantable oximeter with a custom GUI facilitating wireless, real-time, continuous monitoring of SpO<sub>2</sub>, heart rate, and respiratory activity. Encapsulated with a medical-grade silicone layer, the device utilizes a low-modulus, flexible catheter with an optoelectronic sensor that contains two LEDs (645 and 950 nm) and one silicon PD populated by a bendable, miniaturized, battery-powered BLE electronic module (Fig. 3(f)–(i)).

To achieve a more accurate measurement of hemoglobin concentrations using the SRS method, an increasing number of recently built devices have started to employ multiple LEDs and PDs, creating several different source-detector distances in device design.

Rwei et al. [16] proposed a wireless, skin-interfaced biosensor for real-time, continuous monitoring of systemic and

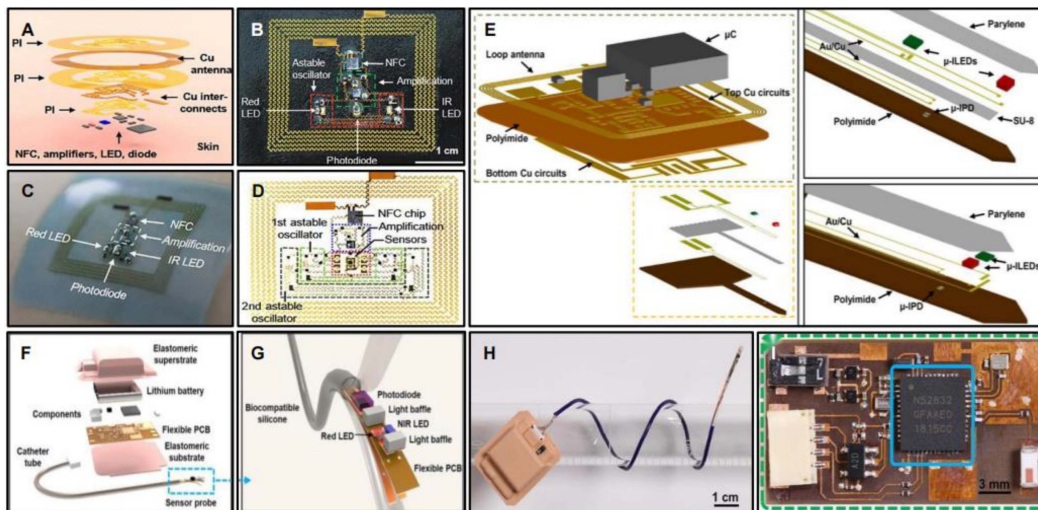


**FIGURE 3.** Wearable NIR devices based on flexible hybrid electronics - devices with single source-detector distance. (a-d) The wireless, battery-free active optoelectronic system with multiple sensing modalities. (a) System with a single LED and photodetector designed for heart rate monitoring and arterial pressure tracking. (b) System with two pulsed LEDs and a single photodetector to monitor peripheral vascular disease. (c) System with two pulsed LEDs, a single photodetector, and colorimetric responsive material for UV dosimetry. (d) System with four pulsed LEDs and a single photodetector for spectrophotometric characterization. [59] Reproduced under the terms of the CC BY-NC 4.0 License. Publisher: AAAS. (e) Miniaturized, fully implantable, wireless probe for  $rStO_2$  measurements. [60] Reproduced under the terms of the CC BY-NC 4.0 License. Publisher: AAAS. (f-i) Implantable, wireless catheter oximeter for real-time monitoring of cardiac physiology in surgical procedures. (f) The electronic module containing a bottom elastomeric substrate, a flexible PCB, a collection of electronic components, a lithium-ion battery, and a top elastomeric encapsulation. (g) Illustration of the sensor probe consisting of a flexible PCB, optical stimulation and sensing components, and optical blocking modules. (h) Image of a catheter oximeter wrapped around a glass rod. (i) Image of an electronic module without encapsulation. [61] Reproduced under the terms of the CC BY-NC 4.0 License. Publisher: AAAS.

cerebral hemodynamics, enabling multi-signal analysis of cerebral oxygenation, cerebral vascular tone, pulse oxygenation, and heart rate. The system, including a laser-defined (ProtoLaser U4, LPKF) fPCB with a Bluetooth low-energy (BLE) system on a chip module and an optical sensor featuring a pair of LEDs (740 and 850 nm) along with an array of silicon photodiodes, defines source-detector distances of 5, 10, 15, and 20 mm for recordings of hemodynamic signals at different tissue depths. With a soft encapsulating PDMS layer on the bottom, this device paves the way for continuous cerebral hemodynamics monitoring for vulnerable pediatric and neonatal patients (Fig. 4(a)).

Wu et al. [62] constructed a non-invasive, self-contained Bluetooth-enabled wireless NIRS probe using red (740nm) and NIR (860nm) LEDs. With two PDs forming source-detector distances at 5 and 10 mm, the device is encapsulated in a skin-safe silicone elastomer with attachment to nonplanar skin tissue facilitated by a thin medical silicone tape (Fig. 4(b)).

Bai et al. [63] proposed an implantable NIRS probe monitoring  $StO_2$  directly within the muscle tissue. Instead of using LEDs, this probe adopts a thin silica-based optical fiber to deliver alternating red (660 nm) and NIR (850 nm) light from external light sources. Thin metal traces connect two micron-scale, silicon-based NPN-type phototransistors supported by a thin narrow polymeric substrate at different distances from the light source. This probe, with bioresorbable barbs made of poly (lactic-co-glycolic acid) [PLGA] serving as anchors

to fix the location, facilitates a low-cost, continuous monitoring, easy-replaceable option for flap oximetry monitoring (Fig. 4(c)).

Similarly, Guo et al. [64] designed a wireless, miniaturized, minimally invasive NIRS probe to continuously monitor  $StO_2$  and  $SpO_2$  in flaps and organ grafts with a bioresorbable barbed structure. Two  $\mu$ -LEDs and two  $\mu$ -PDs enable the SRS method for measuring  $StO_2$  (Fig. 4(d) and (e)). Using the same design, Westman et al. [65] realized continuous, real-time measurement of  $StO_2$  in intercompartmental muscle to monitor lower extremity compartment syndrome.

Although FHE greatly enhanced the wearability of health monitoring devices, the miniaturized device sizes inevitably lead to limited sensing areas, which can be potentially addressed by a hybridized strategy with the modular device design or the construction of sensor networks to be discussed in Section V.

### C. MATERIALS INNOVATION

The advancement in materials science, especially in organic semiconductors, brings the possibility of constructing NIRS devices with intrinsically flexible sensing elements. These NIRS devices usually utilize organic light-emitting diodes (OLEDs) and organic photodiodes (OPDs) fabricated on plastic substrates, leading to soft, organic optoelectronic sensors with great wearability for diverse applications, including pulse oximetry and muscle contraction sensing.

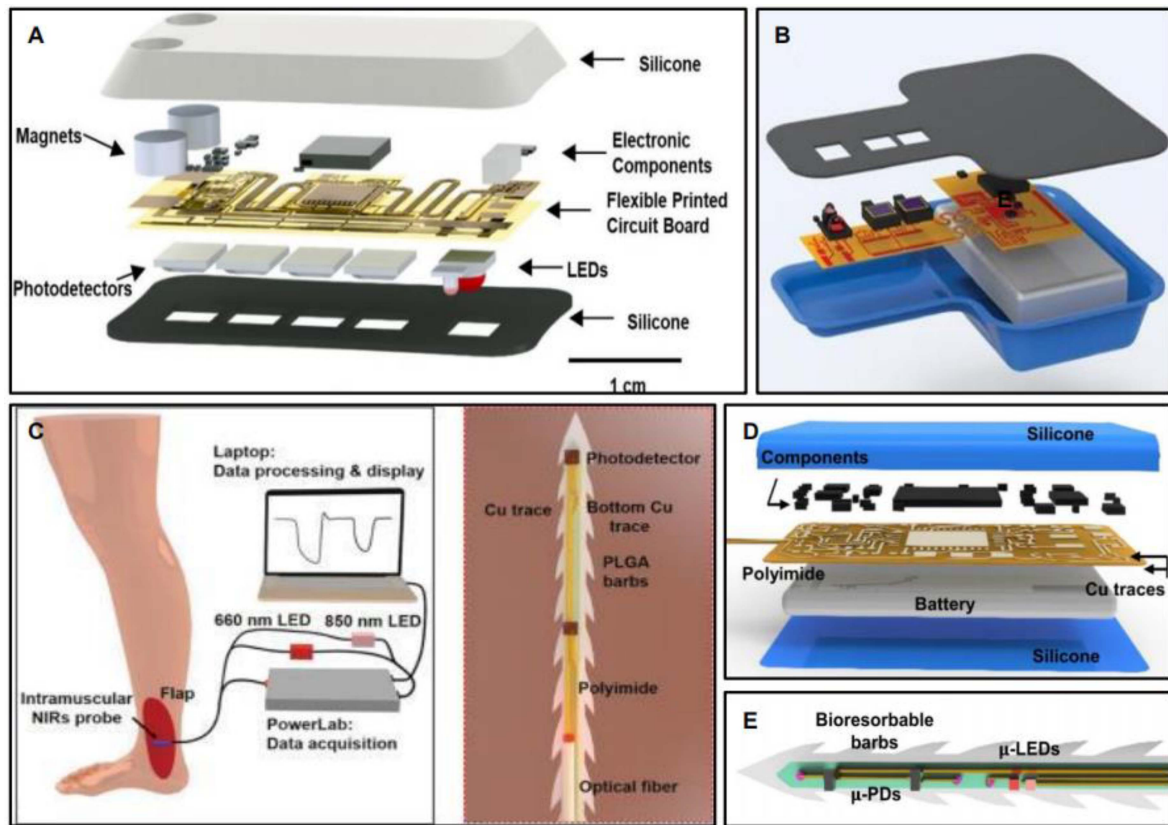


**FIGURE 4.** Wearable NIR devices based on flexible hybrid electronics - devices with multiple source-detector distances. (a) The soft, wireless NIRS device for cerebral hemodynamic monitoring on pediatric subjects containing multiple LEDs and PDs. [16] Reproduced under the terms of the CC BY-NC-ND 4.0 License. Publisher: PNAS. (b) The NIRS sensor for continuous free flap monitoring containing two LEDs and two PDs. [62] Reproduced with permission. Copyright 2022, Thieme. (c) The implantable intramuscular probe for NIRS measurement on muscle flap. [63] Reproduced with permission. Copyright 2022, Thieme. (d-e) The wireless, miniaturized, minimally invasive NIRS probe for continuous monitoring of StO<sub>2</sub> and SpO<sub>2</sub> in flaps and organ grafts. (d) The wireless communication module based on BLE technology. (e) The sensing probe featuring the bioresorbable barb and sensing units containing multiple LEDs and PDs. [64] Reproduced under the terms of the CC BY 4.0 License. Publisher: Springer Nature.

Xu et al. [66] demonstrated epidermal and flexible organic/inorganic hybrid NIR photoplethysmogram (PPG) sensors for cardiovascular monitoring. The sensor consists of a low-voltage, high-sensitivity organic phototransistor sandwiched between polymer layers as the detector and a high-efficiency inorganic LED as the light source, leading to improved power efficiency and enhanced reliability compared to commercial PPG sensors. Thin layers of polyimide (1.8 μm) and PDMS (300 μm) serve as the supporting substrates of the epidermal and flexible sensors, respectively. The epidermal sensor can conformably attach to the skin for reflective PPG, while the flexible sensor can wrap to the finger for transmissive PPG. (Fig. 5(a)–(c))

Khan et al. [17] proposed a flexible printed reflectance oximeter array (ROA) composed of four red (612 nm) and four NIR (725 nm) OLEDs and eight OPDs. The OLED and OPD arrays are stacked together with a source-detector spacing of 0.5 centimeters. A lightweight, comfortable, and wearable sensor platform for muscle assessment based on the ROA is facilitated with an interface to printed EMG or electrocardiography (ECG) electrodes, presenting an unprecedented level of control and integration in printed electronic systems

(Fig. 5(d)–(f)). Based on similar soft optical components, the authors reported a flexible wristband-like two-channel organic optoelectronic sensor with printed red/NIR OLEDs and OPDs. Inkjet-printed silver traces interconnect the optical components with control electronics on a polyethylene naphthalate substrate [67]. They compared three different geometrical arrangements (rectangular, bracket, and circular) of the OLEDs and OPDs. Experimental results indicated that the circular geometry gives the best performance, serving as an instructional guideline for future device design. (Fig. 5(g)–(i)).

However, it has also been reported that solution-processable NIR OLED materials are unstable in the air and show lower efficiencies [68], which is a challenge to be addressed in the development of fully flexible NIRS devices based on intrinsic soft materials.

## V. FUTURE DEVELOPMENT DIRECTIONS

Besides the efforts towards miniature, soft, and wireless NIRS devices using the strategies mentioned above, the future development and application of wearable NIRS will also benefit from the integration with other sensing modalities,

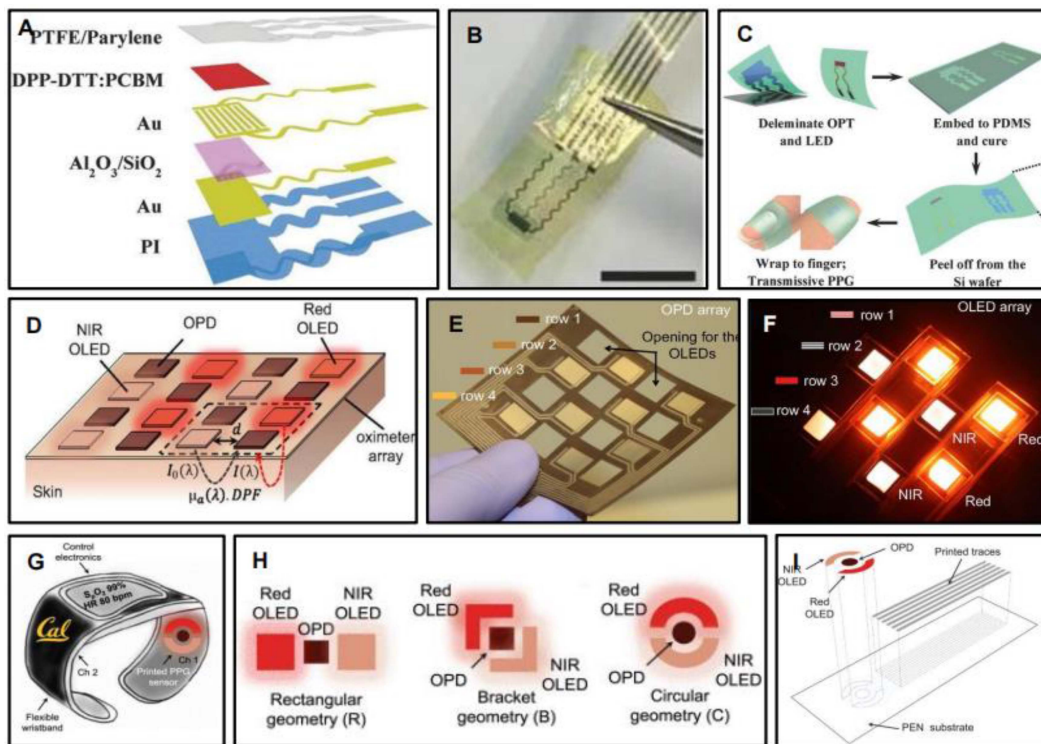


**FIGURE 5.** Wearable NIR devices based on materials innovation. (a-c) The flexible NIR Sensor for cardiovascular monitoring. (a) Schematic of the device structure of the flexible organic phototransistor. (b) Picture of a freestanding phototransistor. (c) Flexible sensor assembly process flow. [66] Reproduced with permission. Copyright 2017, Wiley-VCH. (d-f) The flexible organic reflectance oximeter array (ROA). (d) ROA sensor configuration. (e) OPD array. (f) Red and NIR OLED arrays. [17] Reproduced under the terms of the CC BY-NC-ND 4.0 License. Publisher: PNAS. (g-i) The multi-channel reflectance photoplethysmography sensor. (g) The wearable two-channel organic optoelectronic sensor mounted on the wristband. (h) Different sensor geometries with the same active areas: rectangular geometry, bracket geometry, and circular geometry. (i) Sensor assembly depiction. [67] Reproduced under the terms of the CC BY 4.0 License. Publisher: IEEE.

the advancement in human-machine interface (HMI), the improvement in power source and delivery, and the construction of body area networks (BANs).

The integration of NIRS with other neuroimaging technologies such as functional magnetic resonance imaging (fMRI) [69], [70], [71], EEG [72], [73], [74], positron emission tomography (PET) [75], [76], [77], and magnetoencephalography (MEG) [78], [79], [80], allows multimodal monitoring of physiological states and processes. The integration of NIRS and EEG, for example, facilitates the assessment of hemodynamic activity together with neurovascular coupling [55], [81], [82]. However, the simple combination of two discrete sensors into one system brings the drawbacks of insufficient timing precision and weak synchronization of simultaneous signal recordings [74], [83], [84]. One promising alternative is fully-integrated, or hybrid systems based on complementary metal-oxide-semiconductor (CMOS) microchips [85], [86], [87], [88], [89]. Sensing elements in such fully integrated systems share the same circuit architecture and control module, leading to a reduced time delay between signals and a smaller device footprint.

Wearable NIRS also has huge application potential in advanced HMIs. Its ability to reveal brain activities in different cerebral cortex regions may enable mind reading to control

machines, haptic devices, and robots without physical motions [90]. NIRS signals from local cortical activation can assist the control of robotic mechanical hand orthosis for post-stroke hand recovery and rehabilitation [91]. Together with EEG and EMG, an NIRS-integrated HMI can realize the control of a lower limb rehabilitation training robot to help patients with central nervous system injury do walking training without therapists [92]. The development of wearable NIRS with enhanced accessibility and comfort will facilitate the application of these technologies, as well as broaden its own potential area of application.

Conventional rigid batteries limit the overall mechanical flexibility of wearable NIRS devices. The employment of flexible batteries [93], [94] or even wireless powering techniques, e.g., near-field communication (NFC), would eliminate this restriction. This can also reduce the device size and enhance the wearing comfort for long-term monitoring.

The application of wearable NIRS devices can be further enriched by constructing BANs [95], [96]. BAN is a network of multiple sensors distributed in different body locations for comprehensive continuous health monitoring, which is a revolutionary solution for precision medicine with data-driven decision-making. Miniaturized, soft, and wearable NIRS sensors are good candidates for the sensing nodes of BANs.



The construction of BANs with NIRS sensors distributed over the body would enable simultaneous monitoring of hemodynamics in different body parts. Together with other sensing modalities, it might allow the correlation study of different physiological processes.

## VI. SUMMARY

Recent technological advances have brought the rapid development of wearable NIRS devices. In this review, we introduce the principles of NIRS and summarize typical design strategies for recent NIRS devices, including modular device design, FHE, and materials innovation. We also pinpoint some future development directions that can enhance the applicability and capability of wearable NIRS. We believe the progress and potential of wearable NIRS will benefit the transition towards smart and digital health.

## REFERENCES

- [1] J. A. C. Patterson and G.-Z. Yang, "Ratiometric artifact reduction in low power reflective photoplethysmography," *IEEE Trans. Biomed. Circuits Syst.*, vol. 5, no. 4, pp. 330–338, Aug. 2011.
- [2] Y.-K. Huang, C.-C. Chang, P.-X. Lin, and B.-S. Lin, "Quantitative evaluation of rehabilitation effect on peripheral circulation of diabetic foot," *IEEE J. Biomed. Health Inform.*, vol. 22, no. 4, pp. 1019–1025, Jul. 2018.
- [3] Y.-C. Du, W.-S. Ciou, W.-T. Chen, and C.-M. Tsai, "A novel device for non-invasive assessment of extravasation during injection by NIRS technology," in *Proc. IEEE Sensors*, 2017, pp. 1–3.
- [4] A. Langenfeld et al., "No alteration of back muscle oxygenation during isometric exercise in individuals with non-specific low back pain," *Sci. Rep.*, vol. 12, no. 1, 2022, Art. no. 8306.
- [5] A. M. Feldmann, D. Erlacher, S. Pfister, and R. Lehmann, "Muscle oxygen dynamics in elite climbers during finger-hang tests at varying intensities," *Sci. Rep.*, vol. 10, no. 1, 2020, Art. no. 3040.
- [6] J. Scholz, M. Kohl-Bareis, C. Nolte, C. Hennig, and A. Villringer, "Multivariate spectral analysis of the beat-to-beat sampled cortical NIRS signals and the heart-rate variability," *Proc. SPIE*, vol. 3566, 1998, pp. 106–111.
- [7] J. Menssen, W. Colier, J. Hopman, D. Liem, and C. de Korte, "A method to calculate arterial and venous saturation from near infrared spectroscopy (Nirs)," in *Oxygen Transport to Tissue XXX* (Advances in experimental medicine and biology Series), vol. 645. Berlin, Germany: Springer, 2009, pp. 135–140.
- [8] S. Seddone, L. Ermini, P. Policastro, L. Mesin, and S. Roatta, "Evidence that large vessels do affect near infrared spectroscopy," *Sci. Rep.*, vol. 12, no. 1, 2022, Art. no. 2155.
- [9] R. J. Uilkema and A. B. J. Groeneveld, "Correlates of thenar near-infrared spectroscopy-derived tissue O<sub>2</sub> saturation after cardiac surgery," *Interactive Cardiovasc. Thoracic Surg.*, vol. 6, no. 3, pp. 265–269, 2007.
- [10] C. P. Anderson and S.-Y. Park, "Assessing pulse transit time to the skeletal muscle microcirculation using near-infrared spectroscopy," *J. Appl. Physiol.*, vol. 133, no. 3, pp. 593–605, 2022.
- [11] J. P. DeBlois, W. K. Lefferts, and K. S. Heffernan, "Influence of sprint exercise on aortic pulse wave velocity and femoral artery shear patterns," *Eur. J. Appl. Physiol.*, vol. 120, no. 12, pp. 2635–2647, 2020.
- [12] L. Minati, I. U. Kress, E. Visani, N. Medford, and H. D. Critchley, "Intra- and extra-cranial effects of transient blood pressure changes on brain near-infrared spectroscopy (NIRS) measurements," *J. Neurosci. Methods*, vol. 197, no. 2, pp. 283–288, 2011.
- [13] M. P. Kirschen et al., "Deviations from NIRS-derived optimal blood pressure are associated with worse outcomes after pediatric cardiac arrest," *Resuscitation*, vol. 168, pp. 110–118, 2021.
- [14] F. F. Jöbbsis, "Noninvasive, infrared monitoring of cerebral and myocardial oxygen sufficiency and circulatory parameters," *Science*, vol. 198, no. 4323, pp. 1264–1267, 1977.
- [15] E. M. Frijia et al., "Functional imaging of the developing brain with wearable high-density diffuse optical tomography: A new benchmark for infant neuroimaging outside the scanner environment," *Neuroimage*, vol. 225, 2021, Art. no. 117490.
- [16] A. Y. Rwei et al., "A wireless, skin-interfaced biosensor for cerebral hemodynamic monitoring in pediatric care," *Proc. Nat. Acad. Sci.*, vol. 117, no. 50, pp. 31674–31684, 2020.
- [17] Y. Khan et al., "A flexible organic reflectance oximeter array," *Proc. Nat. Acad. Sci.*, vol. 115, no. 47, pp. E11015–E11024, 2018.
- [18] D. A. Boas, C. E. Elwell, M. Ferrari, and G. Taga, "Twenty years of functional near-infrared spectroscopy: Introduction for the special issue," *Neuroimage*, vol. 85, pp. 1–5, 2014.
- [19] F. Scholkmann et al., "A review on continuous wave functional near-infrared spectroscopy and imaging instrumentation and methodology," *Neuroimage*, vol. 85, pp. 6–27, 2014.
- [20] M. A. Franceschini, S. Fantini, J. H. Thompson, J. P. Culver, and D. A. Boas, "Hemodynamic evoked response of the sensorimotor cortex measured noninvasively with near-infrared optical imaging," *Psychophysiology*, vol. 40, no. 4, pp. 548–560, 2003.
- [21] A. Maki, Y. Yamashita, Y. Ito, E. Watanabe, Y. Mayanagi, and H. Koizumi, "Spatial and temporal analysis of human motor activity using noninvasive NIR topography," *Med. Phys.*, vol. 22, no. 12, pp. 1997–2005, 1995.
- [22] D. A. Boas, K. Chen, D. Grebert, and M. A. Franceschini, "Improving the diffuse optical imaging spatial resolution of the cerebral hemodynamic response to brain activation in humans," *Opt. Lett.*, vol. 29, no. 13, pp. 1506–1508, 2004.
- [23] H. Dehghani, B. R. White, B. W. Zeff, A. Tizzard, and J. P. Culver, "Depth sensitivity and image reconstruction analysis of dense imaging arrays for mapping brain function with diffuse optical tomography," *Appl. Opt.*, vol. 48, no. 10, pp. D137–D143, 2009.
- [24] L. Kocsis, P. Herman, and A. Eke, "The modified Beer-Lambert law revisited," *Phys. Med. Biol.*, vol. 51, no. 5, pp. N91–N98, 2006.
- [25] M. Essenpreis, C. E. Elwell, M. Cope, P. van der Zee, S. R. Arridge, and D. T. Delpy, "Spectral dependence of temporal point spread functions in human tissues," *Appl. Opt.*, vol. 32, no. 4, pp. 418–425, 1993.
- [26] A. Duncan et al., "Measurement of cranial optical path length as a function of age using phase resolved near infrared spectroscopy," *Pediatr. Res.*, vol. 39, no. 5, pp. 889–894, 1996.
- [27] S. J. Matcher, C. E. Elwell, C. E. Cooper, M. Cope, and D. T. Delpy, "Performance comparison of several published tissue near-infrared spectroscopy algorithms," *Anal. Biochem.*, vol. 227, no. 1, pp. 54–68, 1995.
- [28] M. Lindkvist, G. Granåsen, and C. Grönlund, "Coherent derivation of equations for differential spectroscopy and spatially resolved spectroscopy: An undergraduate tutorial," *Spectrosc. Lett.*, vol. 46, no. 4, pp. 243–249, 2013.
- [29] M. Hiraoka et al., "A Monte Carlo investigation of optical pathlength in inhomogeneous tissue and its application to near-infrared spectroscopy," *Phys. Med. Biol.*, vol. 38, no. 12, pp. 1859–1876, 1993.
- [30] S. J. Matcher, P. J. Kirkpatrick, K. Nahid, M. Cope, and D. T. Delpy, "Absolute quantification methods in tissue near-infrared spectroscopy," *Proc. SPIE*, vol. 2389, 1995, pp. 486–495.
- [31] S. Suzuki, S. Takasaki, T. Ozaki, and Y. Kobayashi, "Tissue oxygenation monitor using NIR spatially resolved spectroscopy," *Proc. SPIE*, vol. 3597, 1999, pp. 582–592.
- [32] D. M. Hueber, S. Fantini, A. E. Cerussi, and B. B. Barbieri, "New optical probe designs for absolute (self-calibrating) NIR tissue hemoglobin measurements," *Proc. SPIE*, vol. 3597, 1999, pp. 618–631.
- [33] S. Wojtkiewicz et al., "Self-calibrating time-resolved near infrared spectroscopy," *Biomed. Opt. Exp.*, vol. 10, no. 5, pp. 2657–2669, 2019.
- [34] M. Ferrari and V. Quaresima, "A brief review on the history of human functional near-infrared spectroscopy (fNIRS) development and fields of application," *Neuroimage*, vol. 63, no. 2, pp. 921–935, 2012.
- [35] N. L. Everdell, A. P. Gibson, I. D. C. Tullis, T. Vaithianathan, J. C. Hebden, and D. T. Delpy, "A frequency multiplexed near-infrared topography system for imaging functional activation in the brain," *Rev. Sci. Instrum.*, vol. 76, no. 9, 2005, Art. no. 093705.
- [36] H. Atsumori et al., "Development of wearable optical topography system for mapping the prefrontal cortex activation," *Rev. Sci. Instrum.*, vol. 80, no. 4, 2009, Art. no. 043704.

- [37] M. C. van der Sluijs, W. N. Colier, R. J. F. Houston, and B. Oeseburg, "New and highly sensitive continuous-wave near-infrared spectrophotometer with multiple detectors," *Proc. SPEI*, vol. 3194, 1998, pp. 63–72.
- [38] M. Smith, "Shedding light on the adult brain: A review of the clinical applications of near-infrared spectroscopy," *Philos. Trans. Roy. Soc. Math. Phys. Eng. Sci.*, vol. 369, no. 1955, pp. 4452–4469, 2011.
- [39] G. Greisen, T. Leung, and M. Wolf, "Has the time come to use near-infrared spectroscopy as a routine clinical tool in preterm infants undergoing intensive care?," *Philos. Trans. Roy. Soc. Math. Phys. Eng. Sci.*, vol. 369, no. 1955, pp. 4440–4451, 2011.
- [40] D. T. Delpy, M. Cope, P. van der Zee, S. Arridge, S. Wray, and J. Wyatt, "Estimation of optical pathlength through tissue from direct time of flight measurement," *Phys. Med. Biol.*, vol. 33, no. 12, pp. 1433–1442, 1988.
- [41] E. Gratton, W. W. Mantulin, M. J. vandeVen, J. B. Fishkin, M. B. Maris, and B. Chance, "A novel approach to laser tomography," *Bioimaging*, vol. 1, no. 1, pp. 40–46, 1993.
- [42] M. Cope and D. T. Delpy, "System for long-term measurement of cerebral blood and tissue oxygenation on newborn infants by near infra-red transillumination," *Med. Biol. Eng. Comput.*, vol. 26, no. 3, pp. 289–294, 1988.
- [43] M. J. Herrmann, A.-C. Ehlis, A. Wagener, C. P. Jacob, and A. J. Fallgatter, "Near-infrared optical topography to assess activation of the parietal cortex during a visuo-spatial task," *Neuropsychologia*, vol. 43, no. 12, pp. 1713–1720, 2005.
- [44] A.-C. Ehlis, M. J. Herrmann, A. Wagener, and A. J. Fallgatter, "Multi-channel near-infrared spectroscopy detects specific inferior-frontal activation during incongruent Stroop trials," *Biol. Psychol.*, vol. 69, no. 3, pp. 315–331, 2005.
- [45] A.-C. Ehlis, C. G. Bähne, C. P. Jacob, M. J. Herrmann, and A. J. Fallgatter, "Reduced lateral prefrontal activation in adult patients with attention-deficit/hyperactivity disorder (ADHD) during a working memory task: A functional near-infrared spectroscopy (fNIRS) study," *J. Psychiatr. Res.*, vol. 42, no. 13, pp. 1060–1067, 2008.
- [46] S. F. Husain et al., "Validating a functional near-infrared spectroscopy diagnostic paradigm for major depressive disorder," *Sci. Rep.*, vol. 10, no. 1, 2020, Art. no. 9740.
- [47] H. Kwon et al., "Early detection of cerebral infarction with middle cerebral artery occlusion with functional near-infrared spectroscopy: A pilot study," *Front Neurol.*, vol. 9, 2018, Art. no. 898.
- [48] B. Yang, X. Gu, D. Xu, and C. Fan, "A study on EEG-NIRS testing of drug users' brain function under visual induction," in *Proc. Int. Conf. Comput. Pattern Recognit.*, 2020, pp. 85–89.
- [49] S. Lancia et al., "Trail making test induces prefrontal cortex activation as revealed by a cw wearable-wireless fNIRS/DOT imager," in *Oxygen Transport to Tissue XL (Advances in Experimental Medicine and Biology Series)*, vol. 1072. Berlin, Germany: Springer, 2018, pp. 139–144.
- [50] C.-M. Chen, R. Kwasiński, B. Lo, and G. Z. Yang, "Wearable tissue oxygenation monitoring sensor and a forearm vascular phantom design for data validation," in *Proc. IEEE 11th Int. Conf. Wearable Implantable Body Sensor Netw.*, 2014, pp. 64–68.
- [51] M. Berthelot, C.-M. Chen, G.-Z. Yang, and B. Lo, "Wireless wearable Self-calibrated sensor for perfusion assessment of myocutaneous tissue," in *Proc. IEEE 13th Int. Conf. Wearable Implantable Body Sensor Netw.*, 2016, pp. 171–176.
- [52] M. Berthelot, G.-Z. Yang, and B. Lo, "A self-calibrated tissue viability sensor for free flap monitoring," *IEEE J. Biomed. Health Inform.*, vol. 22, no. 1, pp. 5–14, Jan. 2018.
- [53] W. Guo, X. Sheng, H. Liu, and X. Zhu, "Development of a multi-channel compact-size wireless hybrid sEMG/NIRS sensor system for prosthetic manipulation," *IEEE Sensors J.*, vol. 16, no. 2, pp. 447–456, Jan. 2016.
- [54] K. Gajos, J. Mankoff, C. Harrison, J. McIntosh, A. Marzo, and M. Fraser, "SensIR: Detecting hand gestures with a wearable bracelet using infrared transmission and reflection," in *Proc. 30th Annu. ACM Symp. User Interface Softw. Technol.*, 2017, pp. 593–597.
- [55] A. M. Chiarelli et al., "Fiberless, multi-channel fNIRS-EEG system based on silicon photomultipliers: Towards sensitive and ecological mapping of brain activity and neurovascular coupling †," *Sensors*, vol. 20, no. 10, 2020, Art. no. 2831.
- [56] B. W. Zeff, B. R. White, H. Dehghani, B. L. Schlaggar, and J. P. Culver, "Retinotopic mapping of adult human visual cortex with high-density diffuse optical tomography," *Proc. Nat. Acad. Sci.*, vol. 104, no. 29, pp. 12169–12174, 2007.
- [57] H. Zhao et al., "Design and validation of a mechanically flexible and ultra-lightweight high-density diffuse optical tomography system for functional neuroimaging of newborns," *NueroPhotonics*, vol. 8, no. 1, 2021, Art. no. 015011.
- [58] Y. Ma et al., "Flexible hybrid electronics for digital healthcare," *Adv. Mater.*, vol. 32, no. 15, 2020, Art. no. 1902062.
- [59] J. Kim et al., "Battery-free, stretchable optoelectronic systems for wireless optical characterization of the skin," *Sci. Adv.*, vol. 2, no. 8, 2016, Art. no. e1600418.
- [60] H. Zhang et al., "Wireless, battery-free optoelectronic systems as subdermal implants for local tissue oximetry," *Sci. Adv.*, vol. 5, no. 3, 2019, Art. no. eaaw0873.
- [61] W. Lu et al., "Wireless, implantable catheter-type oximeter designed for cardiac oxygen saturation," *Sci. Adv.*, vol. 7, no. 7, 2021, Art. no. eaabe0579.
- [62] C. Wu et al., "A wireless near-infrared spectroscopy device for flap monitoring: Proof of concept in a porcine musculocutaneous flap model," *J. Reconstructive Microsurgery*, vol. 38, no. 02, pp. 096–105, 2022.
- [63] W. Bai et al., "Intramuscular near-infrared spectroscopy for muscle flap monitoring in a porcine model," *J. Reconstructive Microsurgery*, vol. 38, no. 04, pp. 321–327, 2021.
- [64] H. Guo et al., "Wireless implantable optical probe for continuous monitoring of oxygen saturation in flaps and organ grafts," *Nature Commun.*, vol. 13, no. 1, 2022, Art. no. 3009.
- [65] A. M. Westman et al., "Percutaneously introduced wireless intramuscular near-infrared spectroscopy device detects muscle oxygenation changes in porcine model of lower extremity compartment syndrome," *J. Orthopaedic Res.*, vol. 21, pp. 1011–1017, 2022.
- [66] H. Xu, J. Liu, J. Zhang, G. Zhou, N. Luo, and N. Zhao, "Flexible organic/inorganic hybrid near-infrared photoplethysmogram sensor for cardiovascular monitoring," *Adv. Mater.*, vol. 29, no. 31, 2017, Art. no. 1700975.
- [67] Y. Khan, D. Han, J. Ting, M. Ahmed, R. Nagisetty, and A. C. Arias, "Organic multi-channel optoelectronic sensors for wearable health monitoring," *IEEE Access*, vol. 7, pp. 128114–128124, 2019.
- [68] C. M. Lochner, Y. Khan, A. Pierre, and A. C. Arias, "All-organic optoelectronic sensor for pulse oximetry," *Nature Commun.*, vol. 5, no. 1, 2014, Art. no. 5745.
- [69] H. Mohammadi et al., "Cortical thinning is associated with brain pulsatility in older adults: An MRI and NIRS study," *Neurobiol. Aging*, vol. 106, pp. 103–118, 2021.
- [70] L. Gagnon et al., "Quantification of the cortical contribution to the NIRS signal over the motor cortex using concurrent NIRS-fMRI measurements," *Neuroimage*, vol. 59, no. 4, pp. 3933–3940, 2012.
- [71] H. Sato et al., "A NIRS-fMRI investigation of prefrontal cortex activity during a working memory task," *Neuroimage*, vol. 83, pp. 158–173, 2013.
- [72] S. Fazli et al., "Enhanced performance by a hybrid NIRS-EEG brain computer interface," *Neuroimage*, vol. 59, no. 1, pp. 519–529, 2012.
- [73] B. Koo et al., "A hybrid NIRS-EEG system for self-paced brain computer interface with online motor imagery," *J. Neurosci. Methods*, vol. 244, pp. 26–32, 2015.
- [74] A. Kassab et al., "Multichannel wearable fNIRS-EEG system for long-term clinical monitoring," *Hum. Brain Mapping*, vol. 39, no. 1, pp. 7–23, 2018.
- [75] M. Hiura et al., "Dynamic exercise elicits dissociated changes between tissue oxygenation and cerebral blood flow in the prefrontal cortex: A study using NIRS and PET," in *Oxygen Transport to Tissue XL (Advances in Experimental Medicine and Biology Series)*, vol. 1072. Berlin, Germany: Springer, 2018, pp. 269–274.
- [76] E. Rostrup, I. Law, F. Pott, K. Ide, and G. M. Knudsen, "Cerebral hemodynamics measured with simultaneous PET and near-infrared spectroscopy in humans," *Brain Res.*, vol. 954, no. 2, pp. 183–193, 2002.
- [77] C. Hock et al., "Decrease in parietal cerebral hemoglobin oxygenation during performance of a verbal fluency task in patients with Alzheimer's disease monitored by means of near-infrared spectroscopy (NIRS) — Correlation with simultaneous rCBF-PET measurements," *Brain Res.*, vol. 755, no. 2, pp. 293–303, 1997.
- [78] S. Esterer, L. Abbott, L. Magazzini, and D. McGonigle, "Concurrent tDCS-NIRS-MEG: Insights from a technical pilot," *Brain Stimulation*, vol. 12, no. 2, 2019, Art. no. 497.

- [79] Y. Seki, T. Miyashita, A. Kandori, A. Maki, and H. Koizumi, "Simultaneous measurement of neuronal activity and cortical hemodynamics by unshielded magnetoencephalography and near-infrared spectroscopy," *Proc. SPIE*, vol. 17, 2012, Art. no. 107001.
- [80] B. A. Burke and S. G. Diamond, "Measuring cerebral hemodynamics with a modified magnetoencephalography system," *Physiol. Meas.*, vol. 33, no. 12, pp. 2079–2098, 2012.
- [81] U. Jindal, M. Sood, A. Dutta, and S. R. Chowdhury, "Development of point of care testing device for neurovascular coupling from simultaneous recording of EEG and NIRS during anodal transcranial direct current stimulation," *IEEE J. Transl. Eng. Health Med.*, vol. 3, 2015, Art. no. 2000112.
- [82] M. H. Othman et al., "Resting-State NIRS–EEG in unresponsive patients with acute brain injury: A proof-of-concept study," *Neurointensive Care*, vol. 34, no. 1, pp. 31–44, 2021.
- [83] A. von Lhmann, H. Wabnitz, T. Sander, and K.-R. Müller, "M3BA: A mobile, modular, multimodal biosignal acquisition architecture for miniaturized EEG-NIRS-based hybrid BCI and monitoring," *IEEE Trans. Biomed. Eng.*, vol. 64, no. 6, pp. 1199–1210, Jun. 2016.
- [84] M. Sawan et al., "Wireless recording systems: From noninvasive EEG-NIRS to invasive EEG devices," *IEEE Trans. Biomed. Circuits Syst.*, vol. 7, no. 2, pp. 186–195, Apr. 2013.
- [85] S. Saha, Y. Lu, F. Lesage, and M. Sawan, "Wearable SIPM-based NIRS interface integrated with pulsed laser source," *IEEE Trans. Biomed. Circuits Syst.*, vol. 13, no. 6, pp. 1313–1323, Dec. 2019.
- [86] U. Ha, J. Lee, M. Kim, T. Roh, S. Choi, and H.-J. Yoo, "An EEG-NIRS multimodal SoC for accurate anesthesia depth monitoring," *IEEE J. Solid-State Circuits*, vol. 53, no. 6, pp. 1830–1843, Jun. 2018.
- [87] U. Ha and H.-J. Yoo, "An EEG-NIRS ear-module SoC for wearable drowsiness monitoring system," in *Proc. IEEE Asian Solid-State Circuits Conf.*, 2016, pp. 193–196.
- [88] J. Xu et al., "A 665 nm silicon photomultiplier-based NIRSEEGIT monitoring ASIC for wearable functional brain imaging," *IEEE Trans. Biomed. Circuits Syst.*, vol. 12, no. 6, pp. 1267–1277, Dec. 2018.
- [89] U. Ha et al., "27.2 A 25.2mW EEG-NIRS multimodal SoC for accurate anesthesia depth monitoring," in *Proc. IEEE Int. Solid-State Circuits Conf.*, 2017, pp. 450–451.
- [90] B. Abibullaev, J. An, S. H. Lee, and J. I. Moon, "Design and evaluation of action observation and motor imagery based BCIs using near-infrared spectroscopy," *Measurement*, vol. 98, pp. 250–261, 2017.
- [91] J. Lee et al., "Comparison of feature vector compositions to enhance the performance of NIRS-BCI-triggered robotic hand orthosis for post-stroke motor recovery," *Appl. Sci.*, vol. 9, no. 18, 2019, Art. no. 3845.
- [92] J. Chen, X. Zhang, and R. Li, "A novel design approach for lower limb rehabilitation training robot," in *Proc. IEEE Int. Conf. Autom. Sci. Eng.*, 2013, pp. 554–557.
- [93] X. Xiao et al., "An ultrathin rechargeable solid-state zinc ion fiber battery for electronic textiles," *Sci. Adv.*, vol. 7, no. 49, 2021, Art. no. eabl3742.
- [94] X. Xiao et al., "Advances in solid-state fiber batteries for wearable bioelectronics," *Curr. Opin. Solid State Mater. Sci.*, vol. 26, no. 6, 2022, Art. no. 101042.
- [95] K. Hasan, K. Biswas, K. Ahmed, N. S. Nafi, and M. S. Islam, "A comprehensive review of wireless body area network," *J. Netw. Comput. Appl.*, vol. 143, pp. 178–198, 2019.
- [96] E. Montón et al., "Body area network for wireless patient monitoring," *IET Commun.*, vol. 2, no. 2, pp. 215–222, 2008.